A Solution for Energy-Efficient Operation of Urban Electric Trains: Integrating Rooftop PV with the Active Rectifier in the Traction Substation

An Thi Hoai Thu Anh
Department of Electrical Engineering, University of Transport and Communications, Vietnam
htanh.ktd@utc.edu.vn (corresponding author)

Tran Hung Cuong
Faculty of Electrical & Electronics Engineering, Thuyloi University, Vietnam
cuongth@tlu.edu.vn

Received: 6 December 2023 | Revised: 3 March 2024 | Accepted: 11 March 2024

 DOI: https://doi.org/10.48084/etasr.6709

ABSTRACT

The utilization of renewable sources connected to a grid to reduce traction substation installation costs and electrified trains' operation energy is a highly promising solution in the electric transportation field. This study proposes a DC traction power supply system integrated with a solar energy system using a DC-DC boost converter and an active rectifier replacing a diode located at the traction substation. The active rectifier not only recovers regenerative braking energy when electric trains operate in braking mode but also transfers solar energy from the DC bus to the grid. With the characteristics of urban railway lines utilizing high-power traction motors and high-voltage DC bus, this paper presents the structure of the Modular Multilevel DC-DC boost converter in the solar energy system employing the Maximum Power Point Tracking (MPPT) algorithm, whereas the modular multilevel active rectifier utilizes the Voltage Oriented Control (VOC) algorithm with three loop circuits: phase-lock loop, current loop, and voltage loop. Simulation results in Matlab/Simulink with parameters collected from the Nhon-Hanoi station urban railway line in Vietnam demonstrate that the PV system produces almost 37% of the energy in the accelerating phase of electric trains.

Keywords-modular multilevel DC-DC boost converter; active rectifier; MPPT algorithm; voltage oriented control; PV system

I. INTRODUCTION

The urban railway system is considered one of the crucial solutions to address traffic congestion and reduce environmental pollution in densely populated areas due to its safety, timeliness, and high transport capacity. However, this means of transport is also a significant energy consumer [1]. As a result, numerous energy-saving solutions have been proposed and implemented for the operation of electrified trains on urban railway lines throughout the world. These solutions include regenerative brake energy recovery using energy storage systems located at traction substations or on trains. In [2-3], experimental tests were carried out by installing a wayside supercapacitor energy storage system. The onboard supercapacitors recuperated almost all the regenerative braking energy, saving approximately 12% of the train's energy consumption compared to that utilized by a similar train equipped with braking resistors. In [4], onboard/stationary lithium batteries and supercapacitors were installed on a DC high-speed railway system, and the results exhibited that braking energy recovery can provide significant energy and cost savings. In [5], two 750 VDC prototype reversible substations that were built and tested on a dedicated tramway test track allowed the regeneration of braking energy back into the grid. In [6-7], integrated optimization models on train control and timetable formulation were investigated to allow two trains to exchange braking energy to minimize net consumption rather than dissipate this energy across braking resistors. The efficient train driving strategy tracks the optimal speed curve by applying optimization algorithms to determine optimal speed profiles and the optimal location to place the electric traction substation [7-11]. The use of renewable energy in the power supply system for operating trains was investigated in [12-13].

Solar energy systems have been widely applied in various fields due to their non-polluting nature, lack of noise, and installation ease [14-16]. Several projects have installed PV

panels in urban railway systems worldwide [17-22]. For example, a solar-powered mass transit system was proposed to reduce the total number of vehicles in Pakistan [18]. In [20], a PV system was suggested to be integrated into the Istanbul AirportM1 light metro line for interior lighting. In [21], PVs integrated with supercapacitors in the railway power system were recommended to reduce the total installation cost in a real tramway electric system operating in the city of Naples. In [22], voltage quality and energy saving of PV generation were evaluated in the URT power supply system.

This study proposes a hybrid power supply system and a rooftop PV system combined with an active rectifier located at the traction substation to recover regenerative braking energy and transfer it from the PV system to the grid, as depicted in Figure 1.

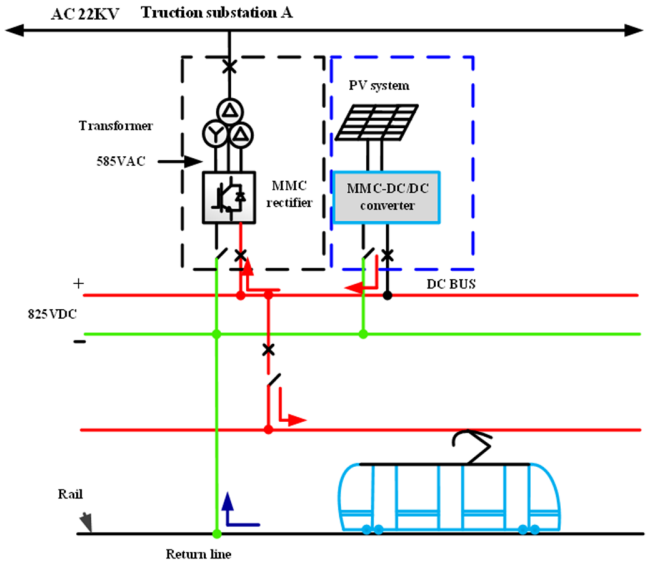

Fig. 1. Integrated rooftop PV.

II. MODELING CONVERTERS

To evaluate the notable advantages of the grid-connected PV system in supporting powering energy for electric trains, the proposed system includes the following components. The electric train operates in accelerating, coasting, and braking modes. The traction substation replaces the diode rectifier with an MMC rectifier capable of bidirectional energy exchange. The PV system connects to the DC bus through a Boost DC-DC MMC converter. This study focuses on modeling and controlling the converters to achieve the stated objectives. In the grid-connected rooftop PV system, there are two converters: an MMC-boost converter connecting the PV to the DC bus and an active rectifier, based on the MMC structure, located at the traction substation. This active rectifier is capable of bidirectional energy exchange to transfer the regenerative braking energy and the PV system energy to the grid.

A. Modeling MMC-Boost DC/DC Converter

Instead of directly transferring energy to the DC bus, the energy of the PV system will pass through an MMC-Boost converter to the DC bus to stabilize the output voltage on the DC bus and to maximize the energy transfer from the PV panels to the output [23]. The MMC-Boost converter is stacked with modules to easily increase the output voltage without using voltage balancing algorithms on capacitors. This reduces the complexity of the configuration and control design [24-26]. The configuration of this converter is essentially the development of the Boost-Buck DC-DC (Figure 2(a)) with outstanding characteristics. Specifically, in a multi-level structure, the current ripple will decrease, enhancing conversion quality. This structure has the advantage of easy construction with compact size, high energy density, and quick response [23]. However, the former still has some drawbacks, such as high starting current and difficulty in voltage adjustment. The converter's input is additionally equipped with an LC filter to limit the continuous current when PV panels achieve low efficiency due to weather conditions.

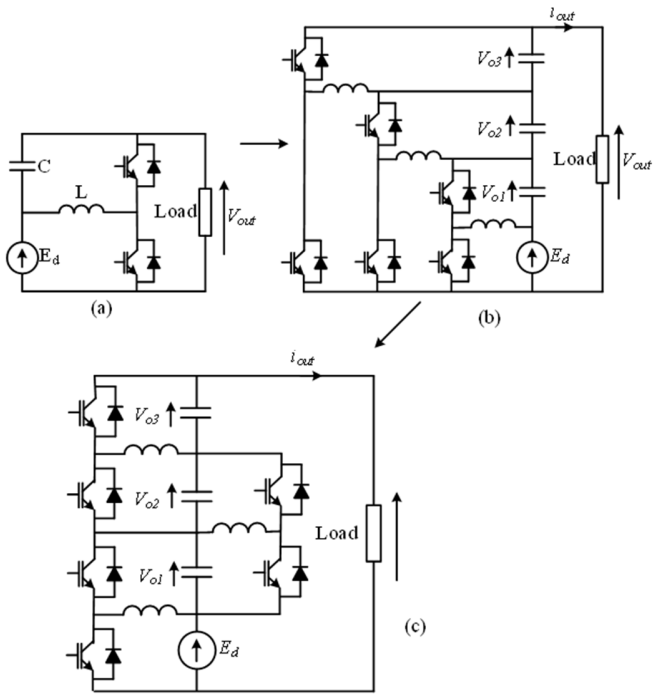

Fig. 2. (a) A modified Buck-Boost DC-DC converter, (b) cascaded topology, (c) a modular three-level modified Buck-Boost converter.

Figure 2(b) portrays the structure of the MMC-Boost converter. The voltage ratio of the converter is given by:

$$\frac{V_{out}}{E_d} = \frac{1}{(1-\alpha)^N} \quad (1)$$

where N is the number of modules and α is the duty cycle. This structure can significantly promote the voltage by integrating multiple layers of modules. The IGBT switching at each layer requires different voltages, for example, the outermost left IGBT in Figure 2(a) must withstand E_d+V_{01}+V_{02}, while the upper switch is only V_{03}. The MMC-Boost Converter structure can also be represented as in Figure 2(c). In this case, the voltage conversion ratio is given by:

$$\frac{V_{out}}{E_d} = 1 + \sum_{i=1}^{N} \frac{\alpha^i}{(1-\alpha)^i} \quad (2)$$

In Figure 2(c), consider the first cell at the bottom including a DC source E_d, the voltage V_{01} on the capacitor connected to E_d, an inductor, and two IGBT valves, 1 and 2. Choose $\alpha = 0.5$ and $V_{01} = E_d$. The second cell includes V_{01} as the input voltage from the source and V_{02} as the output voltage. Therefore, all cells in the converter always have $\alpha = 0.5$. In summary, only the first or last cell needs to be controlled to generate the output voltage of the converter, simplifying the control process. To reduce the current signal's ripple, the Boost-Buck converter topology is improved to a two-phase multilevel MMC-Boost converter with an LC filter at the input of the first cell, as exhibited in Figure 3 [23].

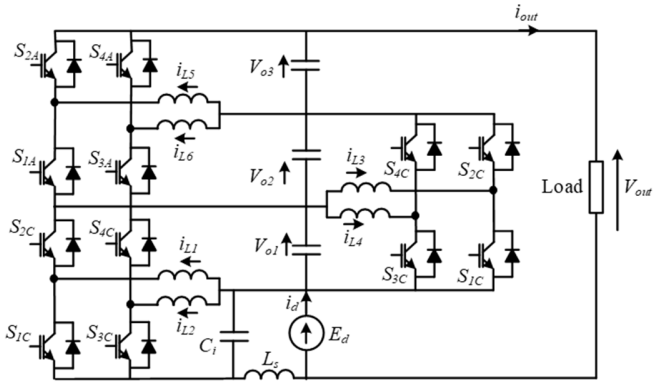

Fig. 3. MMC-Boost Converter with two-phase input LC filtered.

The MMC-Boost converter in Figure 3 operates by cell and sets the α value of the other cells to 0.5. When the top cell is controlled, the valves S_A consist of controlled IGBTs, and the valves S_C maintain their working state unchanged during half a cycle. At this point, the operating state of valve pairs within one cycle is such that when S_1 and S_3 are ON, S_2 and S_4 must be OFF, and vice versa. In this diagram, the valve pairs S_1-S_2 and S_3-S_4 are phased-shifted by 180° so that the current ripple through adjacent coils will mutually cancel out when considered as the input source.

B. Modeling the MMC Rectifier

Aiming at improving the inverters of the electric railway system [27], this converter can provide a stable output voltage and good current quality through appropriate control methods. Compared to other converters, MMC has prominent features in module structure, high efficiency, and low grid current distortion [28-31]. The MMC structure applied to electric trains is crucial, acting as a rectifier to exchange energy between the AC grid and the DC bus of the train [27]. Figure 4 displays an MMC applied to power electric trains. The AC side is connected to the AC grid through a charger, and the DC side is connected to the DC bus. The MMC structure consists of two branches in each phase with N identical submodules connected in series along with the inductor L_o. The submodules are designed as half-bridge converters using IGBT valves to save costs, enhance efficiency, and compact the MMC size [29].

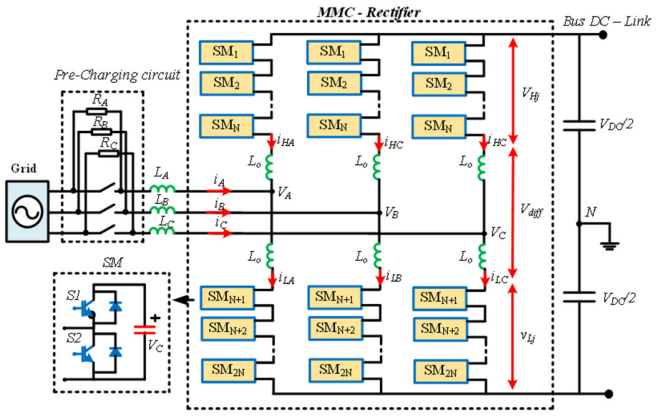

Fig. 4. The circuit structure of the MMC-rectifier.

At the input, additional L_j filters (j = A, B, C), charging circuit R_j, and valves S_j are equipped to ensure technical requirements or circuit disconnection when necessary [27]. The input voltage and current are denoted as v_j, i_j. The upper and lower branch voltages are represented by v_{Hj} and v_{Lj}, while the upper and lower branch currents are i_{Hj} and i_{Lj}. In each phase, there is a circulating current i_{diff_j}. The voltage across each capacitor is V_C, where C_H and C_L are the upper and lower branch capacitors connected to the DC bus. The output of the rectifier ($V_{DC\text{-}bus}$) supplies the DC bus to power the electric train [31]. The relationship between current and voltage in the MMC is described in (3-8):

$$i_j = i_{Hj} - i_{Lj} \quad (3)$$

$$i_{Hj} = i_{diff\_j} + \frac{1}{2} i_j \quad (4)$$

$$i_{Lj} = i_{diff\_j} - \frac{1}{2} i_j \quad (5)$$

$$i_{diff\_j} = \frac{i_{Hj} + i_{Lj}}{2} \quad (6)$$

$$i_j = \frac{v_{Hj} - v_{Lj}}{2} - \frac{1}{2} L_o \frac{di_j}{dt} \quad (7)$$

$$V_{DC\_bus} = v_{diff\_j} + v_{Hj} + v_{Lj} = 2L_o \frac{di_{diff\_j}}{dt} + (v_{Hj} + v_{Lj}) \quad (8)$$

From (8), the output voltage on the DC bus is controlled by the voltage difference between the upper and lower branches of the MMC, and the current i_{diff_j} is controlled by the total voltage across the upper and lower branches of the MMC.

III. DESIGNING THE CONTROL OF THE CONVERTERS

A. Control MMC-Boost Converter

Assuming the input voltage source is constant and there is no current ripple, capacitors are considered ideal. Thus, the output parameters depend on the selected inductance, switching frequency, duty cycle, and input current [23-24]. The output voltage of the proposed converter in Figure 2 is described by:

$$V_{out,N-levels} = E_d + V_{o1} + V_{o2} + \ldots + V_{oN} \quad (9)$$

where the output voltage of each cell is represented as in (8) with the assumption that the value of Ri is 0 for cells other than the first cell.

$$V_{o,each-cell} = \frac{E_d\alpha}{1-\alpha} - \frac{V_Q\alpha}{1-\alpha} - V_D - \frac{I_{out}}{(1-\alpha)^2}\Big(R_i\alpha^2 + R_L + R_Q\alpha + R_D(1-\alpha)\Big) \quad (10)$$

As the input voltage of the subsequent cell is taken from the output voltage of the previous cell, the output voltage of each cell can be calculated by (8). The output voltage of the MMC-Boost converter with 3 levels, depicted in Figure 2, can be expressed by:

$$V_{out,3-levels} = E_d + V_{o1} + V_{o2} + V_{o3} \quad (11)$$

Adjusting the duty cycle of the first cell will result in a wider voltage conversion ratio compared to adjusting the last cell [23]. Therefore, the control of the duty cycle in the first cell will be utilized. Controlling the first cell means that the duty cycle of the first cell changes, while the duty cycle of the other cells is maintained at 0.5. The voltage increment equation for V_{0l} is given by:

$$V_{o1} = \frac{E_d\alpha}{1-\alpha} - \frac{V_Q\alpha}{1-\alpha} - V_D - \frac{I_{out}}{(1-\alpha)^2}\Big(R_i\alpha^2 + R_L + R_Q\alpha + R_D(1-\alpha)\Big) \quad (12)$$

Substituting α by 0.5 and $R_i = 0$ into (12), the output voltage of the second cell can be obtained by:

$$V_{o2} = V_{o1} - V_Q - V_D - XI_{out,2} \quad (13)$$

where:

$$X = \frac{R_L + 0.5R_Q + 0.5R_D}{0,25} \quad (14)$$

For the third cell, the output voltage is given in (15-16). By substituting (13) and (12) into (11), the output voltage of the 3-level converter is given in (18):

$$V_{o3} = V_{o2} - V_Q - V_D - XI_{out,3} \quad (15)$$

$$V_{o3} = V_{o1} - 2(V_Q + V_D) - XI_{out,2} - XI_{out,3} \quad (16)$$

$$V_{out,3-levels} = E_d + V_{o1} + V_{o1} - V_Q - V_D - XI_{out,2} + V_{o1} - 2\big(V_Q + V_D\big) - XI_{out,2} - XI_{out,3} \quad (17)$$

$$V_{out,3-levels} = E_d + 3V_{o1} - 3\big(V_Q + V_D\big) - 2XI_{out,2} - XI_{out,3} \quad (18)$$

By using the same method as the 3-level scheme, the output voltage of the 4-level and 5-level schemes can be obtained as follows:

$$V_{out,4-levels} = E_d + 4V_{o1} - 6\big(V_Q + V_D\big) - 3XI_{out,2} - 2XI_{out,3} - XI_{out,4} \quad (19)$$

$$V_{out,5-levels} = E_d + 5V_{o1} - 10\big(V_Q + V_D\big) - 4XI_{out,2} - 3XI_{out,3} - 2XI_{out,4} - XI_{out,5} \quad (20)$$

where:

$$I_{out,2untilN} = I_{out};\ I_{out,1} = \frac{\alpha}{1-\alpha}I_{out} \quad (21)$$

B. Control MMC-Rectifier

A robust control strategy is necessary to achieve conversion efficiency. In this context, parameters, such as current, voltage on the DC bus, and voltage across the capacitors of each submodule are measured and fed into the control system [27-31]. The appropriate operating states of the MMC are generated through modulation. A simple yet accurate evaluation algorithm for obtaining the DC-bus output voltage was developed:

$$V_{ave\_A} = \sum_{k=1}^{2N} V_{C\_A(k)}/2N \quad (22)$$

$$V_{ave\_B} = \sum_{k=1}^{2N} V_{C\_B(k)}/2N \quad (23)$$

$$V_{ave\_C} = \sum_{k=1}^{2N} V_{C\_C(k)}/2N \quad (24)$$

$$V_{eva} \approx \frac{\big(V_{ave_A} + V_{ave_B} + V_{ave_C}\big)}{3}N \approx \approx \frac{\sum_{k=1}^{2N} V_{C\_A(k)} + \sum_{k=1}^{2N} V_{C\_B(k)} + \sum_{k=1}^{2N} V_{C\_C(k)}}{6} \quad (25)$$

In which, the capacitor voltage of the k^{th} submodule in phase j is represented by $V_{C\_j}(k)$, N is the number of submodules for each branch, V_{ave_j} is the average value of the capacitor voltage for phase j, and V_{eva} is the assessed value of the DC-bus output voltage. The oscillatory components of the capacitor voltage are minimized employing this algorithm. Therefore, voltage sensors at the output are no longer necessary. The noise filtering algorithm for the voltage due to the switching process is presented as:

$$V_{eva\_filter} = \sum_{n=1}^{M} V_{pre(n)}/M \quad (26)$$

V_{eva_filter} is the final value of Bus-V_{DC} to eliminate high-frequency noise components. $V_{eva}(n)$ is the assessed value of Bus-V_{DC} at the n^{th} constant, and M represents the number of samples taken within a long period. Figure 3 shows the structure of the rectifier based on MMC, comprising the evaluation algorithm, closed-loop control of the output voltage, closed-loop control of reactive current splitting, and MMC branch voltage control. The evaluation algorithm is implemented to replace the feedback signal from the high-voltage sensor at the DC output based on (22-26). The control design is carried out in the dq coordinate system with two closed-loop control circuits and a PI controller. The dq-axis components of the grid voltage are considered in the control loop, corresponding to v_d and v_q. $v_{d.ref}$ and $v_{q.ref}$ represent the references for the d and q axes, determined by:

$$v_{d.ref} = v_d + \Big(K_p + \frac{K_i}{s}\Big)\big(i_{d.ref} - i_d\big) + \omega L_f i_q \quad (27)$$

$$v_{q.ref} = v_q + \Big(K_p + \frac{K_i}{s}\Big)\big(i_{q.ref} - i_q\big) - \omega L_f i_d \quad (28)$$

where L_f is the inductance of the filter, and ω is the angular frequency of the grid. The active power and reactive power of the rectifier based on MMC can be calculated by:

$$P = \frac{2}{3}\big(v_d i_d + v_q i_q\big) = \frac{2}{3}v_d i_d \quad (29)$$

$$Q = \frac{2}{3}\big(v_q i_d - v_d i_q\big) = -\frac{2}{3}v_d i_q \quad (30)$$

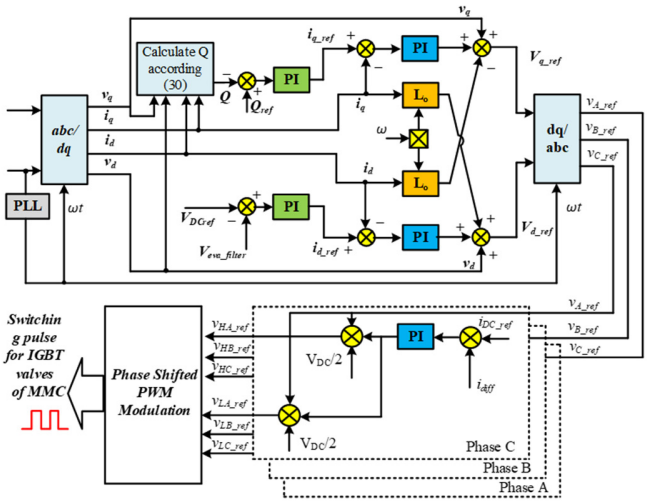

Fig. 5. The control structure of the MMC rectifier.

IV. SIMULATION RESULTS

The train parameters and track alignment data were collected from the urban railway line Nhon-Hanoi Station in Vietnam. The maximum train speed reaches 60 Km/h. This is a 12.5 Km metro line consisting of 12 stations with 8.5 Km elevated with 8 stations and 4 Km underground with 4 stations.

TABLE I. PARAMETERS OF THE ELECTRIC TRAIN

Parameters of electric train	Unit	Value
Train mass (M)	[kg]	192000
Numbers of traction motor (N)		12
Acceleration	[m/s^2]	1
Deceleration	[m/s^2]	1.1
Maximum deceleration during emergency braking	[m/s^2]	1.25
Drag coefficient a	[KN]	0.0115070
Drag coefficient b	[kg/s]	0.0003494
Drag coefficient c	[kg/m]	0.00005497
Wheel diameter (D_{wh})	[m]	0.84
Transmission ratio (i)		3.52:1
Inertial momentum of the train (Jeq)	[kg.m^2]	227.78

TABLE II. PARAMETERS OF THE TRACTION MOTORS

Parameters of IM	Unit	Value
Rated power (P_{nom})	[kW]	180
Rated voltage (U_{nom})	[V]	415
Pairs of pole (Z_p)		2
Power factor ($cos\varphi$)		0.865
Rated speed (n_{nom})	[rpm]	1485
Inertial momentum of the motor(J)	[kg.m^2]	11.2
Inductance of stator (L_s)	[mH]	0.0064
Inductance of rotor (L_r)	[mH]	0.0064
Stator resistance (R_s)	[Ω]	0.008
Rotor resistance (R_r)	[Ω]	0.008

TABLE III. PARAMETERS OF THE MMC- RECTIFIER

Parameters of the MMC rectifier	Unit	Value
Power of rectifier (P_n)	[kW]	2300
Rated voltage (U_n)	[V_{AC}]	585
Grid frequency (f_n)	[Hz]	50
Switching frequency of the MMC rectifier ($f_{swAC/DC}$)	[Hz]	5000
Output voltage after rectifier (U_{DC})	[V_{DC}]	825

TABLE IV. PARAMETERS OF PV SYSTEM AND MMC BOOST CONVERTER OF CAU DIEN STATION

Parameters of PV system	Unit	Value
Maximum power output of a solar panel (P_{pv})	[W]	480
Open-circuit voltage of a solar panel (U_{OC})	[V]	42.71
Short-circuit current of a solar panel (I_{SC})	[A]	14.31
Open-circuit voltage of a solar panel (U_{mp})	[V]	35.38
Current at the maximum power point of a solar panel (I_{mp})	[A]	13.57
PV panels connected in series		9
PV panels connected in parallel		79
The total number of solar panels	Panel	711
Parameters of MMC boost converter		
The number of cells	Cell	3
Switching frequency (f_s)	kHz	20
Input voltage	[V]	528
Output voltage	[V]	825

The PV system is installed at Cau Dien Station, so the train's speed curve is built between the Le Duc Tho and Cau Dien stations, with a train consisting of 12 traction motors in 3 carriages, a distance of 1125m, and a running time within the section of 76s, as observed in Figure 6, including three phases: Accelerating, holding, and decelerating.

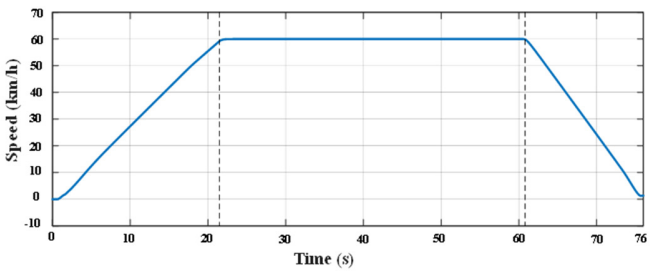

Fig. 6. Operating speed of the electric train in three phases.

The voltage response in Figure 7 demonstrates the voltage control loop circuit controlling the exchange of energy from the source to the load and vice versa in the three phases. The voltage fluctuates at transition points higher than 825 VDC, for example, from 825 VDC to 860 VDC or from 825 VDC to 900 VDC, but then stabilizes at a fixed value of 825V DC.

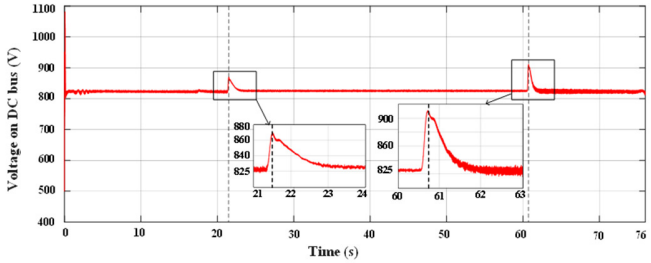

Fig. 7. Voltage on DC bus in 3 phases: accelerating, coasting, and braking.

Figure 8 illustrates the power consumption of the traction motor (P_{IM}), the power obtained from the PV system (P_{pv}), and the power supplied from the grid (P_t). When the grid source is integrated with the PV system, the total energy supplied to the

motors during the accelerating phase (phase A) is additionally supported by the PV system, as the power supplied to the motors is 918 kW from which the grid provides 580 kW and the PV system contributes 338 kW. During the coasting phase (phase BC), the motors obtain power from the PV system only, amounting to 338 kW. During the braking phase (phase CD), the motors operate as generators, returning energy to the grid through the MMC rectifier, including regenerative braking energy and energy from the PV system. Therefore, the energy from the PV system has supported approximately 37% of the total energy in the accelerating phase.

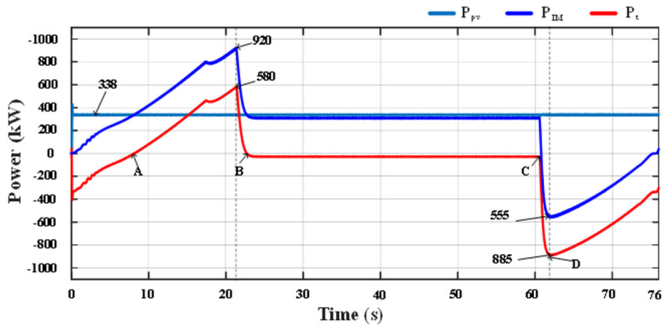

Fig. 8. Power obtained on the transformer (P_t), the motor (P_{IM}), and the PV system (P_{pv}).

Figure 9 presents the responses of the measured current and voltage after the transformer. From the 62nd second, when the braking phase starts, current and voltage are in opposite directions, indicating that the MMC rectifier returns energy to the grid.

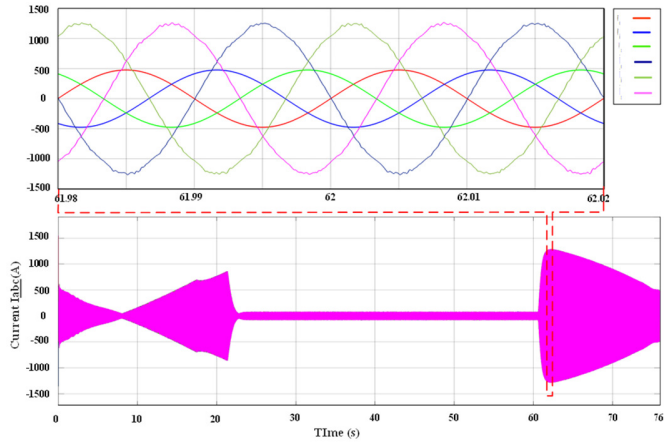

Fig. 9. Current and voltage measured after transformer.

Figure 10 showcases the maximum amplitude of the current measured after the transformer is integrated into the 22kVA power system with a total harmonic distortion of 1.44%, which meets the grid connection standards. These findings reveal that the quality of the controllers achieves good results, responding well to the standards for the system to return energy to the grid.

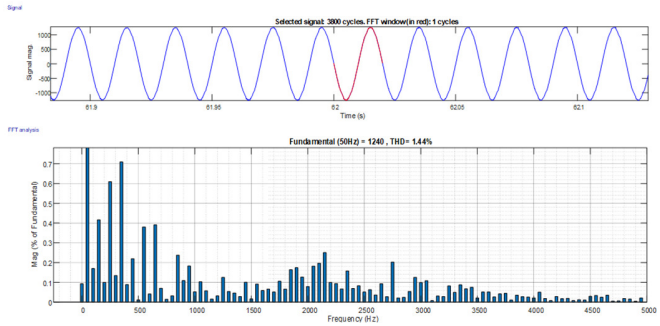

Fig. 10. Total harmonic distortion evaluation at second 62.

V. CONCLUSION AND FUTURE WORK

The current study proposes a promising solution to enhance the advantages of electric railway transportation using hybrid sources: integrating a rooftop PV system at the stations connected to the grid and recovering regenerative braking energy when trains are in the braking phase. This approach deploys the electrical circuit structures of the MMC-Boost converter and MMC-rectifiers suitable for electrified trains that utilize high-power and voltage traction motors. Furthermore, these controllers were designed to support the PV system, while the regenerative braking energy for the grid is up to 37%. This solution not only makes it easier to apply the introduced system to urban electric railways in Nhon-Ha Noi station, but is also feasible for metro lines, both in Vietnam and worldwide.

ACKNOWLEDGEMENTS

This research was funded by the University of Transport and Communications (UTC), Vietnam, under grant number T2024-DT-008.

REFERENCES

[1] M. Popescu and A. Bitoleanu, "A Review of the Energy Efficiency Improvement in DC Railway Systems," *Energies*, vol. 12, no. 6, Jan. 2019, Art. no. 1092, https://doi.org/10.3390/en12061092.

[2] F. Ciccarelli, D. Iannuzzi, K. Kondo, and L. Fratelli, "Line-Voltage Control Based on Wayside Energy Storage Systems for Tramway Networks," *IEEE Transactions on Power Electronics*, vol. 31, no. 1, pp. 884–899, Mar. 2015, https://doi.org/10.1109/TPEL.2015.2411996.

[3] F. Ciccarelli, D. Iannuzzi, and P. Tricoli, "Control of metro-trains equipped with onboard supercapacitors for energy saving and reduction of power peak demand," *Transportation Research Part C: Emerging Technologies*, vol. 24, pp. 36–49, Oct. 2012, https://doi.org/10.1016/j.trc.2012.02.001.

[4] M. Ceraolo, G. Lutzemberger, E. Meli, L. Pugi, A. Rindi, and G. Pancari, "Energy storage systems to exploit regenerative braking in DC railway systems: Different approaches to improve efficiency of modern high-speed trains," *Journal of Energy Storage*, vol. 16, pp. 269–279, Apr. 2018, https://doi.org/10.1016/j.est.2018.01.017.

[5] D. Cornic, "Efficient recovery of braking energy through a reversible dc substation," in *Railway and Ship Propulsion Electrical Systems for Aircraft*, Bologna, Italy, Oct. 2010, https://doi.org/10.1109/ESARS.2010.5665264.

[6] Y. Zhou, Y. Bai, J. Li, B. Mao, and T. Li, "Integrated Optimization on Train Control and Timetable to Minimize Net Energy Consumption of Metro Lines," *Journal of Advanced Transportation*, vol. 2018, Apr. 2018, Art. no. e7905820, https://doi.org/10.1155/2018/7905820.

[7] G. M. Scheepmaker, R. M. P. Goverde, and L. G. Kroon, "Review of energy-efficient train control and timetabling," *European Journal of*

Operational Research, vol. 257, no. 2, pp. 355–376, Mar. 2017, https://doi.org/10.1016/j.ejor.2016.09.044.

[8] T. K. Khoi and N. D. Khuong, "Optimal planning of substations on urban railway power supply systems using integer linear programming," *Transport and Communications Science Journal*, vol. 70, no. 4, pp. 264–278, Oct. 2019, https://doi.org/10.25073/tcsj.70.4.14.

[9] D. D. Tuan and N. D. Toan, "Developing a program to calculate the unitresultant force of trains on Vietnam railways," *Transport and Communications Science Journal*, vol. 71, no. 8, pp. 907–923, 2020.

[10] N. V. Tiem, "Speed control for the train of urban railway using fuzzy-d controller," *Transport and Communications Science Journal*, vol. 71, no. 6, pp. 640–650, 2020.

[11] M. Shravanth Vasisht, G. A. Vashista, J. Srinivasan, and S. K. Ramasesha, "Rail coaches with rooftop solar photovoltaic systems: A feasibility study," *Energy*, vol. 118, pp. 684–691, Jan. 2017, https://doi.org/10.1016/j.energy.2016.10.103.

[12] M. Wei, W. Wei, H. Ruonan, and W. Ziyi, "Auxiliary power supply system of passenger train based on photovoltaic and energy storage," in *2016 IEEE 11th Conference on Industrial Electronics and Applications (ICIEA)*, Hefei, China, Jun. 2016, pp. 784–788, https://doi.org/10.1109/ICIEA.2016.7603688.

[13] L. Piegari, R. Rizzo, I. Spina, and P. Tricoli, "Optimized Adaptive Perturb and Observe Maximum Power Point Tracking Control for Photovoltaic Generation," *Energies*, vol. 8, no. 5, pp. 3418–3436, May 2015, https://doi.org/10.3390/en8053418.

[14] Y. Kassem, H. Gokcekus, and A. Aljatlawe, "Utilization of Solar Energy for Electric Vehicle Charging and the Energy Consumption of Residential Buildings in Northern Cyprus: A Case Study," *Engineering, Technology & Applied Science Research*, vol. 13, no. 5, pp. 11598–11607, Oct. 2023, https://doi.org/10.48084/etasr.6142.

[15] Y. Kassem, H. Gökçekuş, and H. S. A. Lagili, "A Techno-Economic Viability Analysis of the Two-Axis Tracking Grid-Connected Photovoltaic Power System for 25 Selected Coastal Mediterranean Cities," *Engineering, Technology & Applied Science Research*, vol. 11, no. 4, pp. 7508–7514, Aug. 2021, https://doi.org/10.48084/etasr.4251.

[16] P. S. Gotekar, S. P. Muley, and D. P. Kothari, "A Single Phase Grid Connected PV System working in Different Modes," *Engineering, Technology & Applied Science Research*, vol. 10, no. 5, pp. 6374–6379, Oct. 2020, https://doi.org/10.48084/etasr.3746.

[17] H. Hayashiya *et al.*, "Potentials, peculiarities and prospects of solar power generation on the railway premises," in *2012 International Conference on Renewable Energy Research and Applications (ICRERA)*, Nagasaki, Japan, Nov. 2012, https://doi.org/10.1109/ICRERA.2012.6477458.

[18] S. H. I. Jaffery *et al.*, "The potential of solar powered transportation and the case for solar powered railway in Pakistan," *Renewable and Sustainable Energy Reviews*, vol. 39, pp. 270–276, Nov. 2014, https://doi.org/10.1016/j.rser.2014.07.025.

[19] X. J. Shen, Y. Zhang, and Sh. Chen, "Investigation of grid-connected photovoltaic generation system applied for Urban Rail Transit energy-savings," in *2012 IEEE Industry Applications Society Annual Meeting*, Las Vegas, NV, USA, Jul. 2012, https://doi.org/10.1109/IAS.2012.6373995.

[20] B. Kilic and E. Dursun, "Integration of innovative photovoltaic technology to the railway trains: A case study for Istanbul airport-M1 light metro line," in *IEEE EUROCON 2017 -17th International Conference on Smart Technologies*, Ohrid, North Macedonia, Jul. 2017, pp. 336–340, https://doi.org/10.1109/EUROCON.2017.8011131.

[21] F. Ciccarelli, L. P. Di Noia, and R. Rizzo, "Integration of Photovoltaic Plants and Supercapacitors in Tramway Power Systems," *Energies*, vol. 11, no. 2, Feb. 2018, Art. no. 410, https://doi.org/10.3390/en11020410.

[22] D. Feng, H. Zhu, F. Wang, X. Sun, S. Lin, and Z. He, "Evaluation of Voltage Quality and Energy Saving Benefits of Urban Rail Transit Power Supply Systems Considering the Access of Photovoltaics," *CSEE Journal of Power and Energy Systems*, vol. 9, no. 6, pp. 2309–2320, Nov. 2023, https://doi.org/10.17775/CSEEJPES.2020.02320.

[23] R. D. N. Aditama, N. Ramadhani, T. Ardriani, J. Furqani, A. Rizqiawan, and P. A. Dahono, "New Modular Multilevel DC–DC Converter Derived from Modified Buck–Boost DC–DC Converter," *Energies*, vol. 16, no. 19, Jan. 2023, Art. no. 6950, https://doi.org/10.3390/en16196950.

[24] J. Kim and I. Kwon, "Design of a High-Efficiency DC-DC Boost Converter for RF Energy Harvesting IoT Sensors," *Sensors*, vol. 22, no. 24, Jan. 2022, Art. no. 10007, https://doi.org/10.3390/s222410007.

[25] I. Askarian, M. Pahlevani, and A. M. Knight, "Three-Port Bidirectional DC/DC Converter for DC Nanogrids," *IEEE Transactions on Power Electronics*, vol. 36, no. 7, pp. 8000–8011, Dec. 2020, https://doi.org/10.1109/TPEL.2020.3046453.

[26] S. M. Fardahar and M. Sabahi, "New Expandable Switched-Capacitor/Switched-Inductor High-Voltage Conversion Ratio Bidirectional DC–DC Converter," *IEEE Transactions on Power Electronics*, vol. 35, no. 3, pp. 2480–2487, Aug. 2019, https://doi.org/10.1109/TPEL.2019.2932325.

[27] J. Pan, Y. Du, and Z. Ke, "DC-Bus Voltage Sensorless Control of an Active Rectifier with Modular Multilevel Converter," *Energies*, vol. 16, no. 18, Jan. 2023, Art. no. 6569, https://doi.org/10.3390/en16186569.

[28] S. Ji, X. Huang, J. Palmer, F. Wang, and L. M. Tolbert, "Modular Multilevel Converter (MMC) Modeling Considering Submodule Voltage Sensor Noise," *IEEE Transactions on Power Electronics*, vol. 36, no. 2, pp. 1215–1219, Jul. 2020, https://doi.org/10.1109/TPEL.2020.3008524.

[29] K. Tian, B. Wu, S. Du, D. Xu, Z. Cheng, and N. R. Zargari, "A Simple and Cost-effective Precharge Method for Modular Multilevel Converters by Using a Low-Voltage DC Source," *IEEE Transactions on Power Electronics*, vol. 31, no. 7, pp. 5321–5329, Sep. 2015, https://doi.org/10.1109/TPEL.2015.2484222.

[30] D. Ronanki and S. S. Williamson, "Modular Multilevel Converters for Transportation Electrification: Challenges and Opportunities," *IEEE Transactions on Transportation Electrification*, vol. 4, no. 2, pp. 399–407, Jan. 2018, https://doi.org/10.1109/TTE.2018.2792330.

[31] I. Krastev, P. Tricoli, S. Hillmansen, and M. Chen, "Future of Electric Railways: Advanced Electrification Systems with Static Converters for ac Railways," *IEEE Electrification Magazine*, vol. 4, no. 3, pp. 6–14, Sep. 2016, https://doi.org/10.1109/MELE.2016.2584998.